



Toward consistent change detection across irregular remote sensing time series observations

Heather J. Tollerud^{a,*}, Zhe Zhu^b, Kelcy Smith^c, Danika F. Wellington^c, Reza A. Hussain^c, Donna Viola^c

^a U.S. Geological Survey, Earth Resources Observation and Science (EROS) Center, Sioux Falls, SD 57198, USA

^b Department of Natural Resources and the Environment, University of Connecticut, Storrs, CT 06269, USA

^c KBR, Contractor to U.S. Geological Survey, Earth Resources Observation and Science (EROS) Center, Sioux Falls, SD 57198, USA

ARTICLE INFO

Edited by Marie Weiss

Keywords:

Time series analysis
Change detection
CCDC
Landsat
Land use and land cover change

ABSTRACT

The use of remote sensing in time series analysis enables wall-to-wall monitoring of the land surface and is critical for assessing and understanding land cover and land use change and for understanding the Earth system as a whole. However, variability in remote sensing observation frequency through time and across space presents challenges for producing consistent change detection results throughout the available satellite record using approaches such as the Continuous Change Detection and Classification (CCDC) change detection methodology. Here we investigate new modifications to this methodology with the goal of improving accuracy and consistency in results and increasing flexibility for operational usage and future development. The modified method (Band-First Probability, or CCD-BFP) change detection procedure works by calculating a test for each band through time before summarizing between bands. We evaluate the CCD-BFP method compared to an existing implementation of CCDC using a variety of approaches, including a validation dataset of human-interpreted locations, comparison with data from fire events, use of simulated remote sensing data, and qualitative inspection of areas of interest. We find CCD-BFP improves consistency across time and space compared to the existing implementation of CCDC, with more similarity in rates of change across Landsat swath boundaries and before and after the launch of Landsat 7. Also, we find that CCD-BFP detects more of the change events in the validation dataset while reducing the overall number of change detections, indicating that it is able to more accurately capture the most notable land surface change events.

1. Introduction

Comprehensive monitoring of changes on the Earth's surface is crucial for understanding the Earth system. Understanding the causes and consequences of land cover and land use change informs assessments of hazards, global change, food supply, urbanization, and other areas. Information on the specific location and timing of land change is critical for land management and decision support. This information relies on systematic and accurate monitoring enabled by the consistent and continuous collection of remote sensing data with operational missions such as the Landsat satellite program.

Repeated remote sensing observations are essential input data for monitoring the location and timing of land surface change, enabling land change to be observed with high temporal and spatial resolution (Woodcock et al., 2020). Change detection performed on dense satellite time series data has become increasingly feasible in recent years, due to improvements in processing power and data availability (Gómez et al., 2016; Wulder et al., 2018). The 50+ year Landsat

archive provides an extensive and radiometrically consistent record for change detection (Dwyer et al., 2018). However, the availability of observations is not consistent across time and space, with more observations available after the launch of Landsat 7, in swath overlap locations, and in locations with less cloud cover (Egorov et al., 2019). To harmonize across the full record of Landsat, it is important to consider approaches for consistent change detection, with similar detection likelihood throughout but increased confidence and resolution when more data are available.

To improve understanding of land change across the United States, the U.S. Geological Survey has implemented Land Change Monitoring, Assessment, and Projection (LCMAP; Brown et al., 2020). The first data release from LCMAP, LCMAP Collection 1.0 (U.S. Geological Survey, 2020b), used the Continuous Change Detection and Classification (CCDC) algorithm introduced by Zhu and Woodcock (2014). CCDC has two components, change detection and classification. The change

* Corresponding author.

E-mail address: htollerud@usgs.gov (H.J. Tollerud).

detection results serve as input to the classification routine but can also be generated and analyzed independently. The goal of change detection is to identify notable events occurring on the land surface, either associated with a change in land cover or that occur within a particular land cover class. For the purposes of this investigation, we focus on improving the change detection portion of the CCDC algorithm, which we refer to as CCD.

In this study, we present a modification to the CCD method with the goal of improving accuracy and robustness in dealing with differing observation availability. Further benefits of the approach are that it is designed to enable regular use in an operational setting and flexibility for future method development. The modified method is referred to as Band-First Probability (CCD-BFP) and the LCMAP implementation of CCD is referred to as CCD-LCMAP. We provide a brief overview of challenges in the CCD-LCMAP change detection method, outline the set of improvements incorporated in CCD-BFP, and perform an initial evaluation of CCD-BFP performance.

2. Methods

2.1. Change detection algorithm

The CCD-BFP method is a modification of the LCMAP implementation of the CCD change detection algorithm, available at doi:10.5066/P90V8IIX as the Python package `pyccd`. Descriptions of the CCD algorithm are available in publications (Zhu and Woodcock, 2014; Zhu et al., 2015; Xian et al., 2022), and in LCMAP documentation (U.S. Geological Survey, 2020a). Briefly, input data are U.S. Landsat Analysis Ready Data (ARD; Dwyer et al., 2018). A time series of reflectance values is extracted for each 30 m pixel location. The procedure steps forward through dates in the time series, testing for change at each date. The time series for each band is fit up to a date to be tested for change, and the change test is based on a comparison between the measured and predicted reflectance of a set of consecutive Landsat observations.

The CCD-BFP has a different calculation of the change test than CCD-LCMAP. Details of the CCD-BFP algorithm are available in Appendix A. Conceptually, CCD-BFP calculates the probability of a change for each individual Landsat band first and then combines the bands in a final calculation, while CCD-LCMAP calculates a total probability of change by first combining all bands for each individual Landsat observation and then summarizing the observations. The CCD-BFP approach addresses the challenge of outlier Landsat observations by assuming each observation has a set probability of being an outlier. To improve consistency across the varying frequency of available Landsat observations, CCD-BFP enforces a minimum spacing between observations in its change test.

2.2. Evaluation of the algorithm

We utilized multiple approaches to evaluate the CCD-BFP algorithm and compare it to the CCD-LCMAP algorithm. Each evaluation approach has strengths and weaknesses, so the use of multiple approaches to evaluation increases confidence in the robustness of improvements. Evaluation approaches included the following:

- Qualitative inspection of results in locations of interest. Qualitative evaluation of mapped results provided insight into the performance of the approaches, and can show anomalies, for example at the boundary between Landsat swaths. We also looked at rates of change through time to evaluate the effects of differing data availability.
- Comparison against the analyst-interpreted change dataset of Zhu et al. (2020) (see Section 2.2.1). This approach provided quantitative accuracy evaluation.

- Comparison with fire events mapped by interpreters (see Section 2.2.3). Fire events are an especially effective omission error test because they are conspicuous change events over large areas at a known time. Biases in fire detection in areas with topography had been noted by the LCMAP team in qualitative reviews of the product releases, so here we compare fire detection at varying aspect and slope.
- Running CCD on synthetic data with known properties, i.e., simulating very well-behaved Landsat data (see Section 2.2.4). We used simulated data to test for commission error in random data and to test the sensitivity of the approaches for known magnitudes of change.

Evaluation covers the period of the LCMAP CONUS (Conterminous United States) Collection 1.0 products (1985–2017 for products, or 1982–2017 for input data; U.S. Geological Survey, 2020b). This approach allows for direct comparison of CCD-BFP results and released LCMAP products, while still providing a long (33-year) period for analysis. Quantitative evaluations mainly utilized the Time of Spectral Change (SCTIME) LCMAP product, which contains date of change information produced by CCD-LCMAP, but the Primary Land Cover (LCPRI) product was also consulted for context. The LCPRI product contains an eight-class thematic land cover legend.

2.2.1. Change in a set of interpreted locations

For error comparison, we used the validation dataset from Zhu et al. (2020). This dataset contains plot locations that include human-interpreted change events for 1982–2012, refined from Cohen et al. (2016). The causal agent for each event was interpreted using Landsat time series, high resolution images (in Google Earth), and other ancillary data. Causal agents include Harvest, Fire, Stress, Wind, Mechanical, Hydrology, and Other. We focus particularly on Harvest as this is the type of abrupt event that we expect CCD to detect, and also this is the most frequent type of event in the dataset so a substantial sample is available.

We ran both CCD-LCMAP and CCD-BFP on Landsat time series data for the plot locations in this dataset and recorded the total number of change detections found in 7222 plot time series. Omission error is calculated as the fraction of the change events in the database that do not have a matched CCD change detection occurring within ± 1 year of the change period in the database. We used the offset of ± 1 year because we are more interested in the broad performance of the algorithm than in the details of small interpreter/CCD disagreements. We exclude Structural Decline and Growth/Recovery change types from overall error calculations as CCD targets abrupt change as opposed to more gradual processes.

We calculated commission disagreement as the fraction of changes detected by CCD that did not occur within ± 1 year of a change event period in the dataset. We refer to this as commission disagreement instead of commission error because we expect that there could be events on the ground that are associated with a substantial change in the surface reflectance and yet do not meet the definition of change used by the interpreters. For example, ecosystems affected by drought might have lasting shifts in species composition with no change in land cover class. We expect commission disagreement to be a combination of this definition uncertainty and commission error in the sense that change was detected despite no substantial change in surface reflectance.

We also ran CCD-BFP across the dataset using a range of alternative threshold cutoff values for the probability of change (from 10^{-5} through 10^{-15}) to investigate the sensitivity of the CCD-BFP algorithm.

2.2.2. Landsat data

For evaluating the CCD-BFP algorithm performance with remote sensing data, we used Landsat Collection 1 U.S. ARD (U.S. Geological Survey, 2020c) as input data. We accessed the archive of Landsat Collection 1 used as input data for LCMAP and retrieved observations

between the launch of Landsat 4 in 1982 and December 31, 2017 (the time range of LCMAP Collection 1.0 input data). Multiple Landsat ARD tiles of CCD-BFP results were produced in the course of evaluating the CCD-BFP algorithm, as well as smaller subsets and sample sites. Results from the Landsat ARD tiles h03v09, h12v15, and h14v09 are discussed in the results section.

We randomly selected 4000 “chip” locations to compare change frequency across CONUS. There are 892 852 100 pixel \times 100 pixel (3 km \times 3 km) chips entirely within the LCMAP CONUS footprint; we assigned random numbers to all and then selected the first 4000 chips from the LCMAP archived copy of the Landsat Collection 1 dataset.

2.2.3. Fire severity evaluation

To evaluate algorithm performance in detecting events that cover more area than a single 30 m location, we utilized fire data from Monitoring Trends in Burn Severity (MTBS, [U.S. Geological Survey, 2021](#)). We plot agreement between MTBS and CCD rather than error because MTBS is not intended as a validation dataset, and the definition of change is not necessarily the same for CCD and MTBS. However, large disagreements are expected to generally be errors in CCD rather than MTBS because creation of MTBS products involved human interpreters. We downloaded CONUS Burn Severity Mosaics for the years 1985–2017 and extracted all pixels flagged as low, moderate, or high severity within the area of the Landsat ARD tile h03v09 (located in California), which was selected as it had a variety of mapped fires throughout the study period. We also downloaded CONUS Burned Areas Boundaries datasets for 1985–2017 and extracted fire ignition date for all of the burned locations in h03v09. The ARD tile h03v09 was selected as it had a variety of mapped fires from throughout the study period. Fire pixels were considered to agree if a CCD change detection occurred within ± 2 years of the ignition date of the fire. To compare fire change detection across varying land surface topography, we used the 30 m slope and aspect datasets utilized as ancillary data for LCMAP land cover classification ([U.S. Geological Survey, 2020a](#)).

2.2.4. Simulated data

We simulated multi-band time series data to evaluate algorithm performance when the time series behavior is fully understood. To produce simulated data, normally distributed noise was added to a constant value (reflectance of 0.15, scaled to 1.5×10^3 for input to pyccd), optionally with a change in the constant value at a known time. All bands utilized for change detection were simulated with the same underlying pattern and the same standard deviation for the added random noise, but with different noise values. The standard deviation used was 0.02 in units of reflectance, to allow for a range of simulated change magnitudes both more and less than the standard deviation. Simulated observations were generated at a Landsat-like frequency of one every 16 days, with no simulated masked or cloud observations.

To evaluate commission error, we developed four synthetic datasets for comparing the performance of the CCD-LCMAP and CCD-BFP algorithms. Each dataset was produced with 100 000 simulated time series. The “basic” dataset had uncorrelated noise. The “autocorrelation” dataset had autocorrelation in the noise values for observations near each other in time, but with fully independent bands. The “correlated bands (all)” dataset was produced with correlation between the noise values for the bands for each date, and the “correlated bands (visible/SWIR)” dataset was produced with correlation between the blue/green/red bands and between the two SWIR (shortwave infrared) bands.

We produced simulated time series with changes in the reflectance to test the sensitivity of the CCD versions. We produced time series with change of varying magnitude (reflectance change of 0 to 0.1) and at a range of different dates (0 to ~ 13 years), with 100 simulated time series for each combination of change magnitude and change date.

Table 1
Number of validation changes detected by CCD.

	Validation changes	Changes detected	
		CCD-LCMAP	CCD-BFP
Harvest	1048	698 (67%)	791 (75%)
Mechanical	332	209 (63%)	211 (64%)
Fire	184	108 (59%)	134 (73%)
Hydrology	77	54 (70%)	51 (66%)
Wind	14	6 (43%)	11 (79%)
Total detections		4893	4312

2.3. Processing details

The implementation of both CCD-LCMAP and CCD-BFP was based on the pyccd code used in LCMAP, written in Python. The qualitative Landsat evaluation data were run on the U.S. Geological Survey (USGS) Denali supercomputer ([USGS Advanced Research Computing, 2022](#)). Mapping and spatial analysis was done in QGIS ([QGIS Development Team, 2016](#)), change accuracy calculations were done in Julia ([Bezanson et al., 2017](#)), and some analysis of LCMAP Collection 1.0 data was done using the Interactive Data Language 8.7 (IDL) programming language and ENvironment for Visualizing Images 5.5 (ENVI) geospatial analysis software from Harris Geospatial Solutions.

For comparisons of the ARD tile h03v09 and qualitative comparisons of CONUS locations, we utilized LCMAP Collection 1.0 products as the CCD-LCMAP version for comparison to CCD-BFP because the algorithm and input date ranges are the same for LCMAP Collection 1.0 and the CCD-BFP run. We re-ran the 4000 random chip locations with CCD-LCMAP in order to compare processing times.

We used a Landsat scene boundary shapefile from [U.S. Geological Survey \(2018\)](#) to categorize locations as either scene center or swath overlap. For the 4000 random chips, we categorized the entire chip as either scene center or swath overlap based on the center of the chip.

3. Results

The CCD-BFP method generally identified more of the events in the validation dataset of [Zhu et al. \(2020\)](#) than the CCD-LCMAP method, while having fewer total change detections across all plots in the dataset (Table 1). The total detections are all changes detected by CCD in the 7222 plots in the validation dataset, including those associated with Stress or Other events and those not associated with any event in the validation dataset. More changes were identified by CCD-BFP than by CCD-LCMAP for four of the five abrupt change categories (Harvest, Mechanical, Fire, and Wind). More Hydrology changes were identified by CCD-LCMAP than by CCD-BFP. For the largest category of change (Harvest), varying the threshold for change detection in CCD-BFP produced a well-behaved relationship, with an increase in commission disagreement associated with a reduction in omission error (Fig. 1). Both omission error and commission disagreement were reduced in CCD-BFP compared to CCD-LCMAP.

Fewer changes were flagged by CCD-BFP than CCD-LCMAP in the 4000 chips randomly distributed across CONUS. CCD-LCMAP detected 37 430 730 changes in the 4000 chips and CCD-BFP detected 30 160 935 changes ($\sim 19\%$ fewer). This result indicates that CCD-BFP, with the current threshold, is less sensitive to change overall despite detecting more of the change events in the validation dataset. This is potentially positive because excessive sensitivity to spectral change can increase the risk of misclassification and mischaracterization of land change in the subsequent assignment of land cover types.

The potential for observational bias in CCD-LCMAP was noted previously by [Brown et al. \(2020\)](#). Indeed, locations in the random dataset saw increased change detection frequency with CCD-LCMAP after the Landsat 7 launch in 1999 and also a decrease in change detection frequency in 2012 (when only Landsat 7 data were available; Fig. 2).

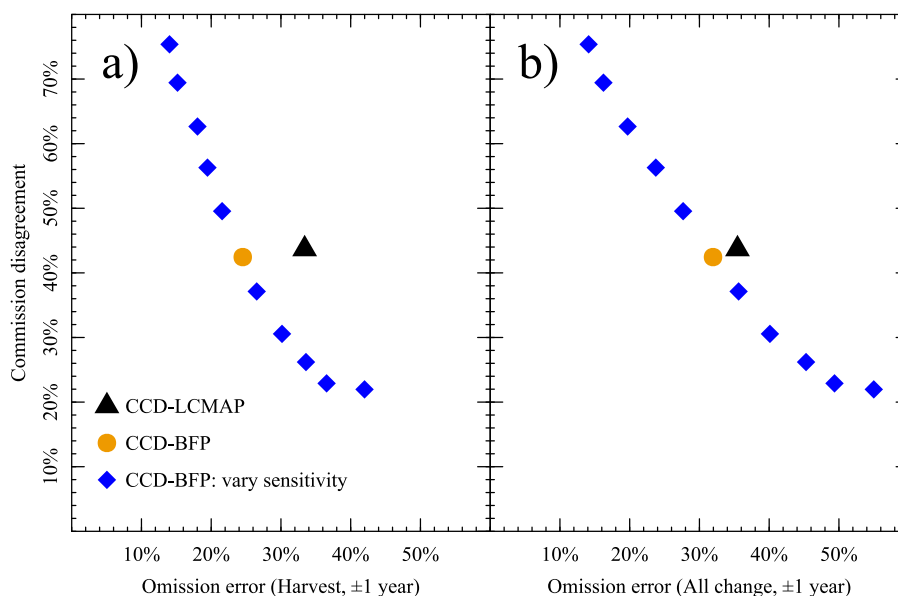


Fig. 1. Omission error compared to commission disagreement for different versions of CCD in the full set of validation plot locations. Omission error is for (a) harvest events and (b) all change. An event marked in the dataset is considered to be omission error if a CCD change detection does not occur within ± 1 year of the event date range. A change event in CCD is considered to be commission disagreement if it does not occur within ± 1 year of an event date range. See also Supplement Table B.3 for data values.

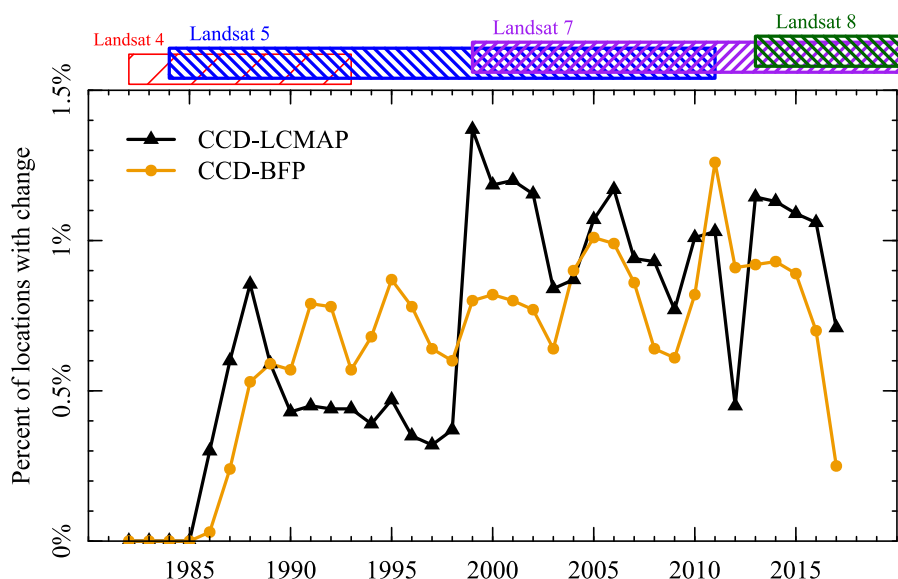


Fig. 2. Change detection through time for CCD-LCMAP and CCD-BFP. Both versions of CCD were run within 4000 randomly selected chip locations from across CONUS. For each year the percentage of 30 m locations with change was calculated for each chip, and then summarized across chips by plotting the value for the median chip. Years with data availability for Landsats 4, 5, 7, and 8 are shown at the top.

However, in CCD-BFP, change detection occurred with a more similar frequency before and after 1999, with a slight increase in change detections through time. For both, change detection was decreased in the final year (2017) due to not having enough observations to confirm change at the end of the time series. Extending the time series with data after 2017 would be expected to increase change detections in 2017.

Fewer changes were detected early in CCD-BFP, especially in scene center locations, with more detections in CCD-LCMAP than CCD-BFP for 1985–1988 despite lower detection frequency for the rest of the pre-Landsat 7 era (1989–1998). Omission error was higher for 1985–1988 for CCD-BFP than CCD-LCMAP, although both had high omission error compared to later years (Table 2). For the rest of the validation study period, omission error was substantially lower for CCD-BFP than CCD-LCMAP, for both scene center and swath overlap locations. The omission error rate was more consistent between time periods and

swath locations for CCD-BFP (range: 16.8% to 22.5%) than for CCD-LCMAP (range: 22.1% to 48.3%). The CCD-LCMAP omission error for 1989–1998 in swath overlap locations was particularly high (48.3%), which is notable because observation availability is expected to be generally similar for 2000–2011 in scene center (22.1% omission error). Swath overlap locations for 2000–2011 have the highest (post-1988) omission error for CCD-BFP (22.5%), suggesting that the CCD-BFP approach is not entirely consistent in its treatment of differing observation densities, although it is a substantial improvement over CCD-LCMAP.

Commission disagreement was slightly lower on average for CCD-BFP than for CCD-LCMAP. Although CCD-LCMAP commission disagreement was quite uniform across time and between scene center and swath overlap (range: 42.2% to 43.6%), CCD-BFP commission disagreement was higher for 1989–1998 and lower for 2000–2011. The validation dataset has ~39% more events per year in the period 2000–2011

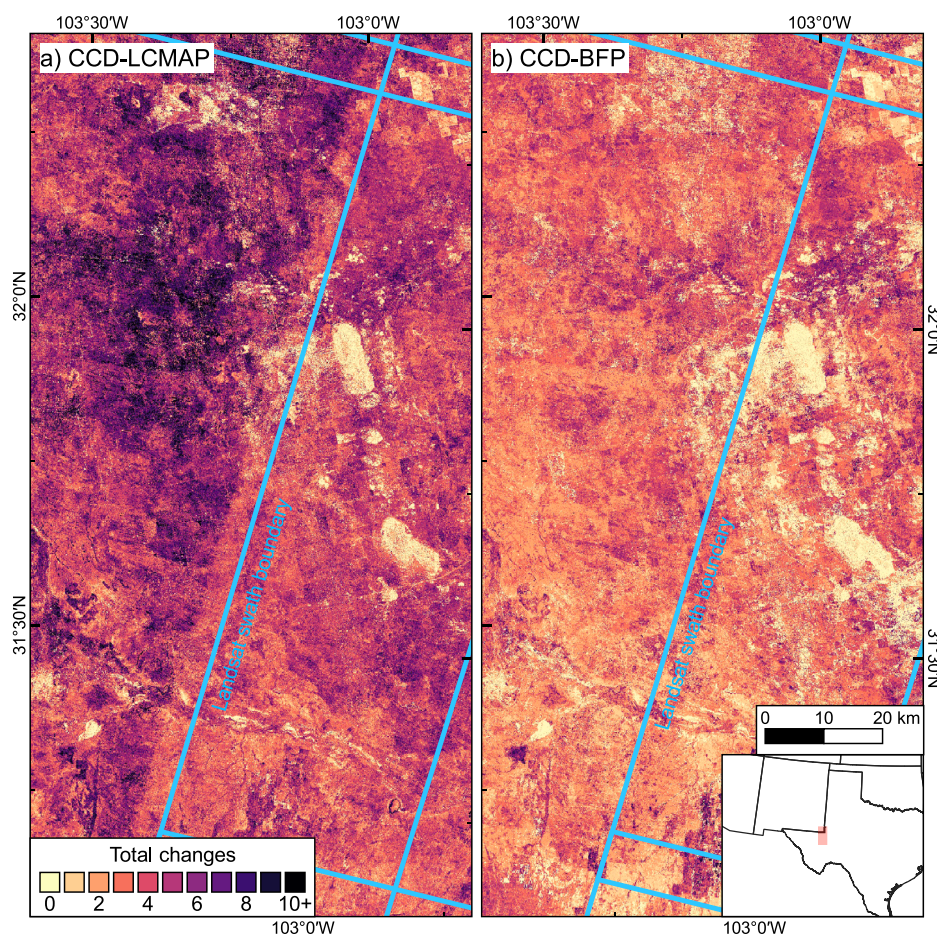


Fig. 3. Number of change detections through the study period (1985–2017) per 30 m location for a site in a western Texas, USA, that is dominated by semiarid grass/shrub. Change detections related to precipitation are common in the region. Approximate Landsat scene boundaries are shown as light blue lines; the line running down the center of each image depicts a swath boundary between scene center (west) and swath overlap (east). Total number of change detections shown for (a) CCD-LCMAP and (b) CCD-BFP. (For interpretation of the references to color in this figure legend, the reader is referred to the web version of this article.)

Table 2
Omission error and commission disagreement for change in the validation dataset.

	Years	Harvest omission error		Commission disagreement	
		CCD-LCMAP	CCD-BFP	CCD-LCMAP	CCD-BFP
Scene center	1985–1988	55.7%	64.6%	50.5%	45.5%
	1989–1998	32.7%	19.3%	42.2%	48.3%
	2000–2011	22.1%	16.8%	43.4%	38.9%
Swath overlap	1985–1988	38.2%	39.7%	45.4%	43.5%
	1989–1998	48.3%	18.6%	43.6%	48.2%
	2000–2011	29.6%	22.5%	42.9%	34.5%
Both	1984–1988	47.6%	53.1%	48.0%	44.4%
	1989–2012	30.9%	19.7%	43.2%	42.3%

than in 1989–1998, a pattern that is not seen in the LCMAP reference data-based change estimates (Pengra et al., 2021; Auch et al., 2022). This indicates that the increased commission disagreement for CCD-BFP in 1989–1998 might be attributable to reduced event identification in the validation dataset.

In the LCMAP Collection 1.0 products, features were visible in the pattern of change detection along the Landsat swath boundaries in some locations, particularly in the grasslands of the Great Plains (Brown et al., 2020). These locations tend to have frequent change detections that are associated with drought. These swath boundary features were not prominent in these locations for CCD-BFP (Fig. 3). In Fig. 3, change detection was higher on the scene center side of the swath boundary in CCD-LCMAP; in other Great Plains locations (generally, farther north)

we observed reduced change detection rates along the swath edge but similar rates in the scene center and the swath overlap (Fig. 4). In CCD-BFP we observed locations where change detection rates appeared to be different between scene center and swath overlap, but we did not observe any sharp lines at swath boundaries. Artifacts were noticeable perpendicular to the Landsat swath in a few areas in both CCD-LCMAP and CCD-BFP, related to data gaps due to the Landsat 7 scan-line corrector (SLC) failure (e.g., in the southwestern portion of Fig. 3).

The pattern of change across CONUS was broadly similar between CCD-BFP and CCD-LCMAP (Fig. 5a). Both versions of CCD had the highest rates of change detection in southern CONUS grass/shrub locations, with additional high change rates in the Southeast, in areas with substantial tree cutting activities. However, CCD-BFP had substantial shifts in rate of change across much of CONUS (Fig. 5b). In CCD-BFP the rates of change were decreased compared to CCD-LCMAP in high change grass/shrub areas, but increased in the Northeast, which had very low change rates in CCD-LCMAP.

The CCD-LCMAP method varies in detection of fire across surface slope and aspect. Higher severity fires are more likely to be detected by CCD-LCMAP (change within ± 2 years of the ignition date), but within a given severity, change detection is substantially decreased on north-facing slopes compared to south-facing slopes (Fig. 6). Comparing the low severity fires by slope, north-facing locations have very low numbers of change detections in CCD-LCMAP on steeper slopes (Fig. 7a), although change detections are highest for south-facing locations when slopes are moderately steep ($20^\circ - 35^\circ$).

With CCD-BFP, fire detection frequency is generally increased over CCD-LCMAP for all slopes and aspects. Most notably, agreement for low

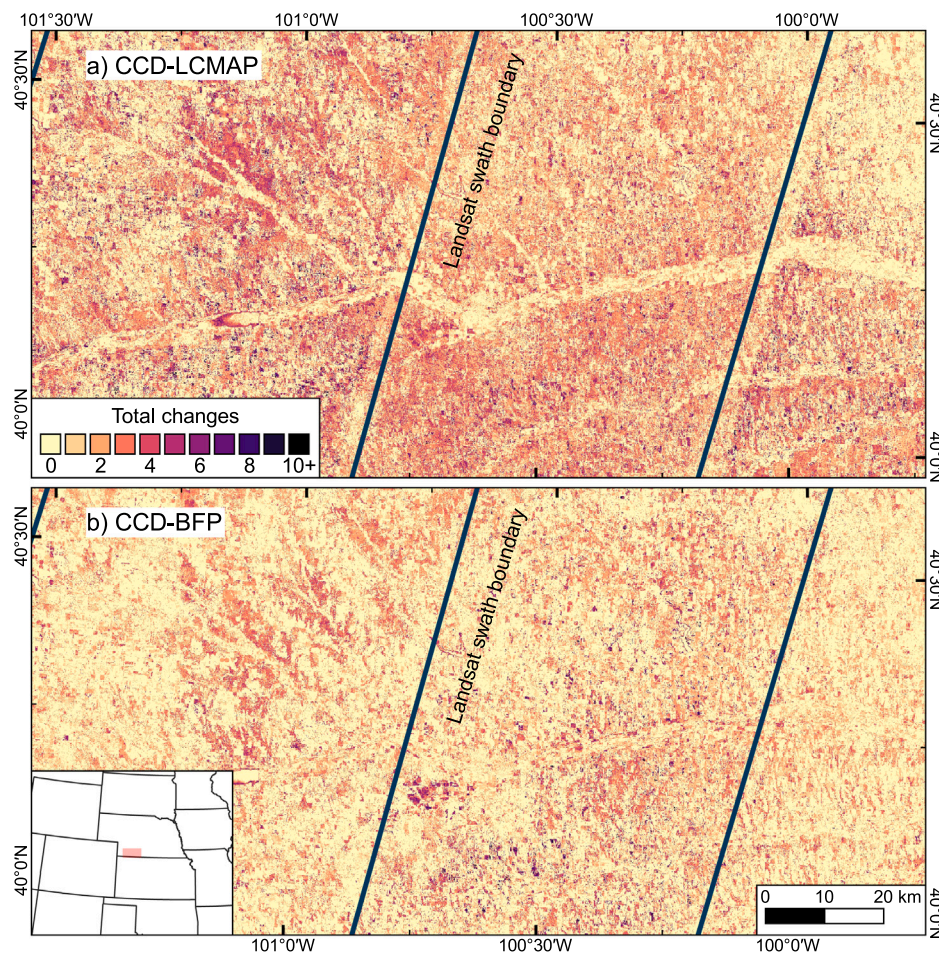


Fig. 4. As in Fig. 3, number of change detections through the study period (1985–2017) per 30 m location for a site in southern Nebraska, USA. This site is also semi-arid grass/shrub, with a substantial amount of cropland. Scene line artifacts visible in CCD-LCMAP are not seen in CCD-BFP.

severity fire is increased from near 0% to almost 50% on steep north-facing slopes (Fig. 7b). As in CCD-LCMAP, in CCD-BFP fire detection is reduced on north-facing slopes compared to south-facing slopes, but to a lesser extent, especially for moderate and high severity fires (Fig. 6). Unlike CCD-LCMAP, CCD-BFP tends toward higher agreement on steeper slopes (up to $\sim 40^\circ$) for both south- and north-facing locations. Both approaches have reduced agreement on the steepest slopes ($> 40^\circ$), but these represent a small fraction of the MTBS fire detections ($< 3\%$).

Commission error for simulated data was much higher for CCD-LCMAP than for CCD-BFP (Fig. 8). Commission error in CCD-LCMAP was highest immediately after 1 year (when most of the simulated time series initialized and change testing began). A secondary peak in commission error occurs at approximately 1.4 years (observation 32), which is the expected time of the first re-fit of the regression model. The full time series commission error rate for CCD-LCMAP was moderate compared to rates of land cover conversion change for basic, uncorrelated simulated data (0.17%), but up to an order of magnitude higher for correlated simulated data (0.41%, 0.99%, and 2.24% for visible/SWIR correlation, all band correlation, and autocorrelation, respectively). For CCD-BFP, the basic and correlated bands tests had no commission error. The only test with substantial commission error in CCD-BFP was the all bands correlation test, with 0.46% full time series commission error, with the highest rates of commission error around 2 years of elapsed time. The CCD-BFP autocorrelation test had three change detections out of the 100,000 test runs (0.003% commission error).

4. Discussion

Accuracy in detection of change events is improved over CCD-LCMAP in CCD-BFP with a reduced number of total change detections. The reduction in omission error is quite substantial after the early period (through 1988; Table 2).

Consistency across scene boundaries is improved in CCD-BFP, with scene boundary lines reduced in the Great Plains (Figs. 3 and 4) and no sudden and substantial jump in change detection when Landsat 7 data are added to the time series (Fig. 2). Although patterns are broadly similar across CONUS, CCD-BFP is more uniform in change detection rate across space, with fewer change detections in the southern Great Plains and more in the Northeast (Fig. 5). Given the reduced omission error, qualitative observations of increased detection of wind event related changes in the North, and the difficulty of interpreting the high levels of change in the southern Great Plains in CCD-LCMAP, the more uniform level of change detection across CONUS in CCD-BFP is likely to indicate an improvement in consistency of detecting change.

The reduced detection of fire on north-facing slopes seen in CCD-LCMAP is improved in CCD-BFP (Fig. 6). The near-complete lack of low severity fire change detection on steep north-facing slopes in CCD-LCMAP (Fig. 7) is notable, especially the sharp difference at almost directly east or west. Although CCD-BFP has some remaining differences between south- and north-facing slopes, the elimination of the sharp difference and crossover between steep and less steep slopes indicates that CCD-BFP is less biased in this way.

The CCD-BFP change detection method is able to improve change detection accuracy while switching to a band-first calculation. The

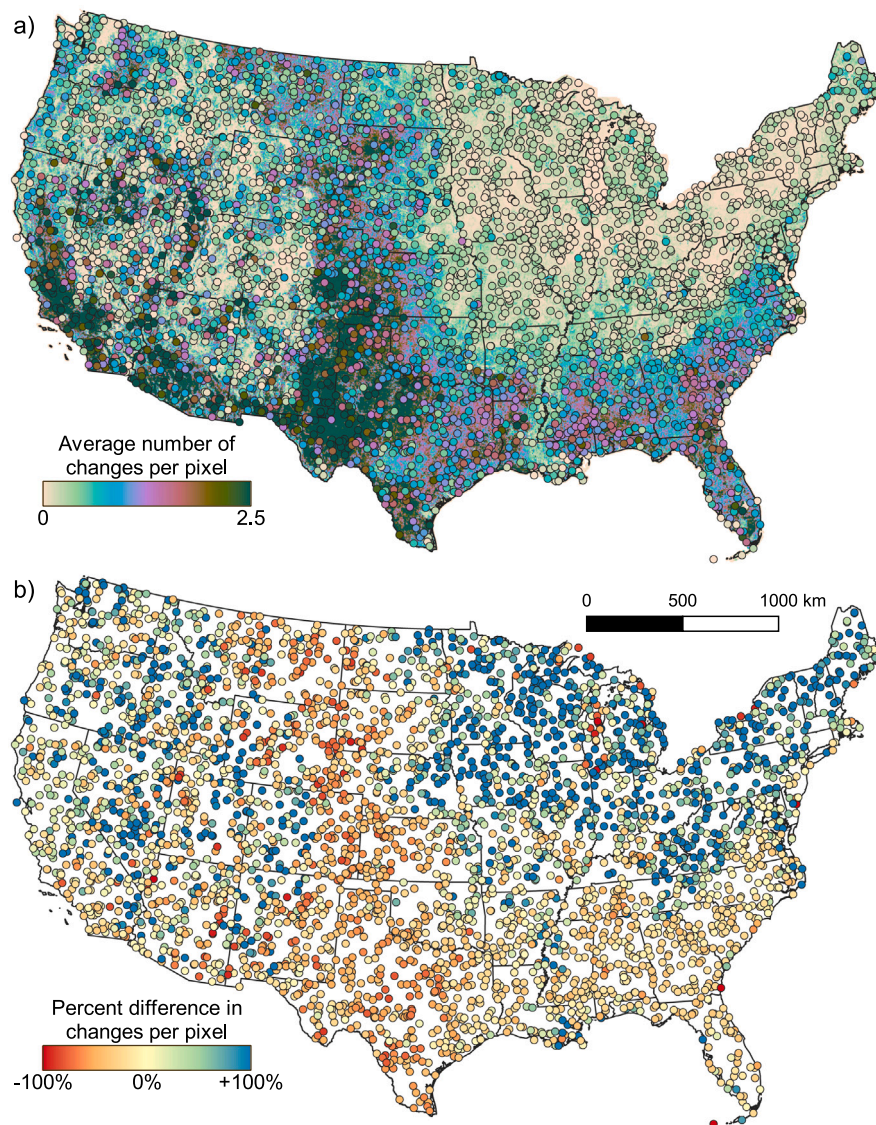


Fig. 5. Comparison of number of changes in CCD-LCMAP and CCD-BFP throughout the study period (1985–2017). Average changes per pixel are calculated for 100 pixel \times 100 pixel (3 km \times 3 km) chips. All chips in CONUS are shown for CCD-LCMAP and 4000 randomly selected chips are shown for CCD-BFP. (a) Average number of changes per pixel for CCD-BFP (circles) and CCD-LCMAP (underlying map). (b) Percent difference in changes per pixel from CCD-LCMAP to CCD-BFP ($\frac{\text{BFP-LCMAP}}{\text{LCMAP}}$), where red represents more changes in CCD-LCMAP compared to CCD-BFP, and blue represents more changes in CCD-BFP compared to CCD-LCMAP. (For interpretation of the references to color in this figure legend, the reader is referred to the web version of this article.)

band-first approach provides several advantages. The probability calculation for a single band is more straightforward than the sum of multiple bands, which allows for easier analysis and more complex statistical approaches. The band-first approach also has the potential for incorporating additional data sources collected on a different temporal schedule. Because the band probabilities are calculated first and then combined, an additional source might be incorporated into the last step even if the observations were from a different set of dates.

The masking approach used in CCD-BFP also has potential for future use. A single value is used in CCD-BFP to represent the probability that an observation is clear, but future investigation could vary this value or incorporate a confidence level produced by a masking routine.

Although overall accuracy and consistency are increased in CCD-BFP compared to CCD-LCMAP, some areas of concern highlight trade-offs in the CCD approach to change detection, and are areas of potential future research. For one, processing time is increased in CCD-BFP (by approximately a factor of 6) due to the calculation of multiple permutations of possible observations. Processing time can be expected to scale up with increased input data.

Another area of concern is that sensitivity for change detection increases through time in CCD-BFP, while it is relatively flat in CCD-LCMAP (Fig. B.10). This varying sensitivity allows CCD-BFP to have very low commission error due to random noise (Fig. 8), but reduces change detection early in the record and means that long models will detect change when a similar magnitude event would not be detected in a short model. A time-dependent sensitivity adjustment was not included in CCD-BFP in order to analyze the change detection power and commission rate without it, but in the future it might be desirable to investigate a sensitivity adjustment that would increase commission error for short models and reduce power to detect change for long models, but would be more consistent through time.

Qualitatively, we observed that locations that convert from land cover that has high reflectance variability to land cover with low reflectance variability are a challenge for the forward processing approach of CCD. A notable example is the development of cropland. It is difficult to detect this type of change because in the change test only a limited time series is used to represent the possible new model, and reflectance variability is difficult to calculate reliably across a short time series, especially with autocorrelation and outliers.

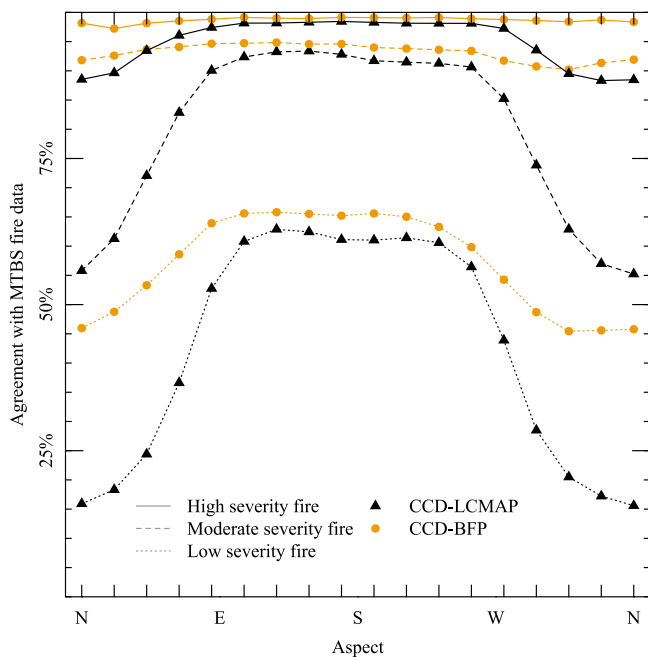


Fig. 6. Percentage of burned pixels in MTBS products with a change detected by CCD within ± 2 years, by aspect. Detection of fire events is increased in CCD-BFP over CCD-LCMAP, especially on north-facing slopes. This figure incorporates 2.5×10^7 pixels (U.S. Landsat ARD tile h03v09) with 3625384 burned pixel locations. Low severity fire (dotted lines), moderate severity fire (dashed lines), and high severity fire (solid lines) are shown. Burned pixels in flat locations (slope $< 5^\circ$) are not included.

Several challenges remain that CCD-BFP does not address, that might be addressed by future work. The interaction between drought and change detection is important, especially in grass/shrub locations. Grassland reflectance can be substantially increased in visible wavelengths during drought but then quickly return to expected reflectance after receiving precipitation. This behavior is expected in a grassland, so the desirability of detecting these types of changes within a land cover change detection method such as CCD is dependent on user requirements. In CCD-BFP, these types of change detections are reduced in some areas compared to CCD-LCMAP, but still occur at a high rate.

5. Conclusions

The CCD-BFP method is an improvement over CCD-LCMAP in several ways, including reduced omission error, improved consistency, and increased method flexibility. Detection of known events is increased while overall change rates are reduced. Sharp differences in change detection rate in CCD-LCMAP after the launch of Landsat 7 are reduced in CCD-BFP, as are boundary lines between overlap and scene center regions in the southern Great Plains. The method also improves operational ease of use for calculating updates. Further method improvements and parameter tuning have the potential to improve accuracy and allow for incorporation of additional data sources.

CRedit authorship contribution statement

Heather J. Tollerud: Conceptualization, Methodology, Software, Validation, Writing. **Zhe Zhu:** Validation, Data curation, Writing – review & editing. **Kelcy Smith:** Software, Writing – review & editing. **Danika F. Wellington:** Validation, Writing – review & editing. **Reza A. Hussain:** Software. **Donna Viola:** Validation, Writing – review & editing.

Declaration of competing interest

The authors declare that they have no known competing financial interests or personal relationships that could have appeared to influence the work reported in this paper.

Data availability

LCMAP data and code available as described in text and citations.

Acknowledgments

We thank Jessica Walker and two anonymous reviewers whose valuable comments and suggestions improved this manuscript.

Funding was provided by the National Land Imaging Program that is part of the Core Science Systems Mission Area of the U.S. Geological Survey. The contribution to this work by KBR employees was supported under contract 140G0121D0001. Zhe Zhu was supported by USGS Great Plains Cooperative Ecosystem Studies Unit (CESU) Program for Improving Land Cover Classification and Land Change Detection for LCMAP (#G19AC00365) and the USGS-NASA Landsat Science Team Program for Toward Near Real-time Monitoring and Characterization of Land Surface Change for the Conterminous US (140G0119C0008). Any use of trade, firm, or product names is for descriptive purposes only and does not imply endorsement by the U.S. Government.

Appendix A. CCD-BFP algorithm description

A.1. CCD initialization and fitting

For the initial steps of data preparation, removal of data containing clouds and snow, and initialization, CCD-BFP uses the same methods as CCD-LCMAP. Briefly, time series data are read for each location in the Landsat ARD Albers Equal Area coordinate grid within the area of interest. The Landsat Quality Assessment band is used to screen the time series for cloud, cloud shadow, and snow. Each time series is analyzed starting over an initial span of data that passes empirical checks for stability, before iterating through additional data to test for change.

In CCD-LCMAP, the basis for change detection is a comparison between a fitted model of the Landsat time series through a specific date, and several subsequent Landsat observations. The equation used for fitting the time series model is

$$\hat{y}_i(t) = c_{0i} + c_{1i}t + \sum_{j=1}^3 \left(a_{ji} \cos \frac{2\pi jt}{T} + b_{ji} \sin \frac{2\pi jt}{T} \right) \quad (\text{A.1})$$

where $\hat{y}_i(t)$ is the predicted value for the i th Landsat band at date t ; c_{0i} , c_{1i} , a_{ji} , and b_{ji} are fitted coefficients; and T is the number of days per year. The second (third) order harmonics are not included until 18 (24) Landsat observations are included in the model. Five Landsat bands (green, red, near infrared, and the two SWIR bands) are used for change detection, because the blue and thermal Landsat bands were not found to improve results.

Because improving the calculation of the change test is the purpose of CCD-BFP, in this paper we use a time series modeling approach that is broadly similar to CCD-LCMAP. However, a few modifications to the modeling approach are required to support the CCD-BFP change test. In CCD-LCMAP, the model is fit using Least Absolute Shrinkage and Selection Operator (LASSO). In CCD-BFP, Ordinary Least Squares (OLS) is used. Iteratively re-fitting the model after incorporating non-change observations is computationally expensive but has been shown to improve accuracy (Zhu et al. 2020). In this regard, CCD-BFP breaks with CCD-LCMAP by favoring recalculation of regression coefficients with every new observation, rather than at progressive intervals. CCD-BFP uses a cumulative computational approach to reduce the required

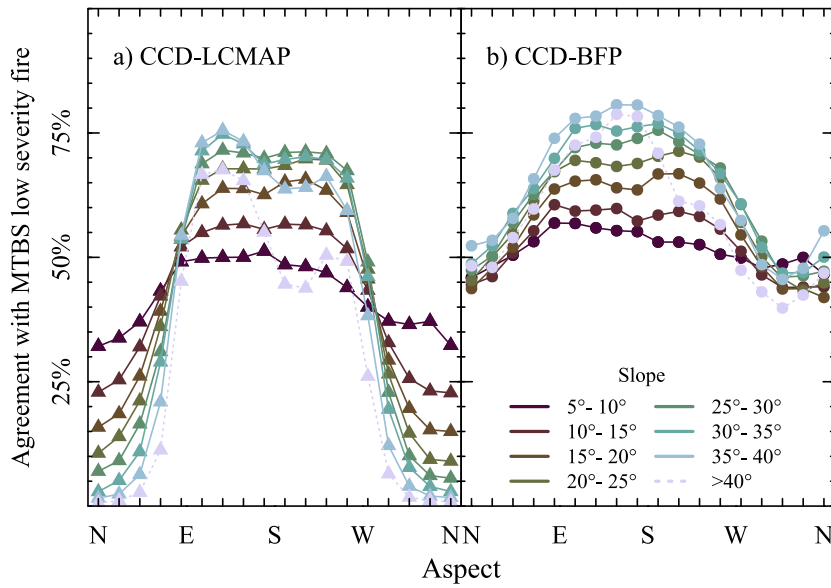


Fig. 7. Percentage of low severity burned pixels in MTBS products with a change detected by CCD within ± 2 years. This figure incorporates 2.5×10^7 pixels (U.S. Landsat ARD tile h03v09) with 1 809 353 burned pixel locations. Results are shown for (a) CCD-LCMAP and (b) CCD-BFP. Each line is agreement for a range of slope values, with lighter shades for steeper slopes. Agreement for flat areas (slope $< 5^\circ$) is 52.0% for CCD-LCMAP and 60.7% for CCD-BFP.

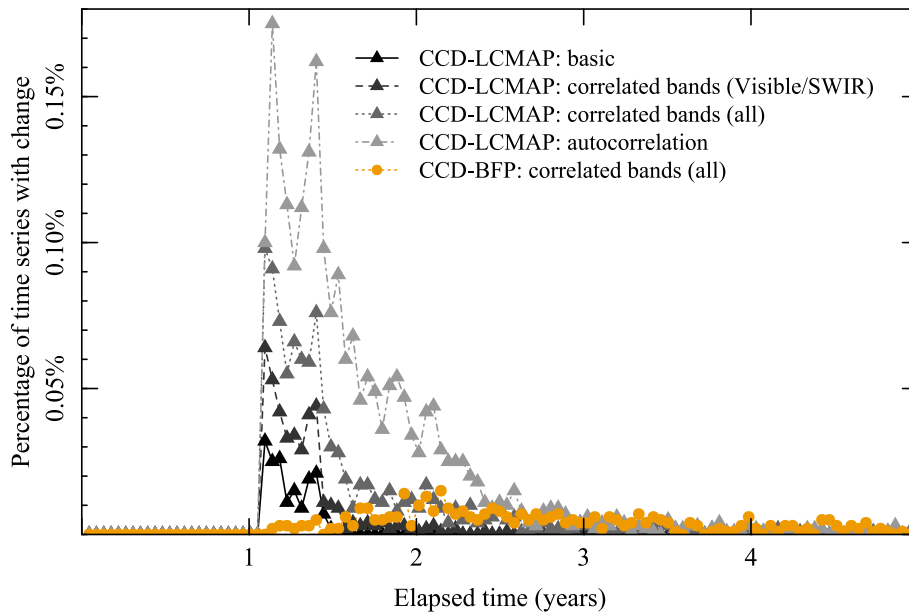


Fig. 8. Percentage of simulated time series with commission error through time (out of 100 000 simulated time series). The time of the change detections is shown on the x-axis. The “basic” simulated data have a uniform reflectance with normally distributed noise. The “correlated bands (visible/SWIR)” simulated data have correlated noise values for all the visible bands, and correlated noise values for the two SWIR bands. The “correlated bands (all)” simulated data have correlated noise values for all bands, and the “autocorrelation” simulated data have temporal autocorrelation. Note that CCD-BFP had no change detections for basic or correlated bands (visible/SWIR), and only 3 out of 100 000 for autocorrelation simulated data.

processing time. This computational approach is described in more detail in Appendix C.

A.2. Calculation of the change test in CCD-LCMAP

The main focus of the CCD-BFP modification is on the method used to decide whether a set of new observations is consistent with the fitted model, or if they are different enough to be flagged as change. First, we will describe the CCD-LCMAP change test and considerations for modifying it, followed by the new change test method.

Change is detected in CCD-LCMAP when multiple consecutive observations after the end of the fit (Eq. (A.1)) exceed a threshold. Let \mathbb{M}

be the set of dates for m observations that are compared to the fit. The change test for CCD-LCMAP is

$$\min_{t \in \mathbb{M}} \left(\sum_{i=1}^{\mu} \frac{(y_i(t) - \hat{y}_i(t))^2}{\max(s_{i,24}^2, \alpha_i^2)} \right) > \chi_{0.99}^2(\mu) \quad (\text{A.2})$$

where $y_i(t)$ is the observed value for the i th Landsat band at date t , $\mu = 5$ is the number of bands used for change detection in CCD-LCMAP, and $s_{i,24}$ is the root mean square error (RMSE) of the 24 observations that are nearest by day of year for the current model fit of the i th band. The value $\chi_{0.99}^2(\mu)$ is used as the threshold for change detection.

A major advantage of this approach is that the change test is quite robust to observations that are problematic (for example, clouds that

were not filtered by Fmask). Summing first across the bands aggregates measurements from a problematic observation, and using the minimum observation for the test prevents extreme outlier observations from having a disproportionate effect on results. Robustness to outlier observations is a critical attribute for the change test because even the most accurate remote sensing datasets have error. Even a relatively low number of outlier observations is a challenge for a change test that is designed to detect change based only on a few observations, particularly when there are multiple consecutive outliers. Multiple consecutive outliers can be expected to occur due to random chance, but also might be temporally correlated (e.g., a persistent weather pattern with smoke or clouds that are difficult to detect). An alternative change test needs to maintain this robustness to outliers.

One challenge with the CCD-LCMAP change test is that the sensitivity to change is not constant through time. The peek number and change threshold modifications at the beginning of a time series run are meant to equalize the sensitivity to change between locations, but do not correct for sensitivity through time. In addition, anomalies can occur along the edge of a Landsat swath where minor orbital drift produces locations that are in the overlap zone at some times but outside it during others (see Figs. 3 and 4).

The CCD-LCMAP change test is semi-empirical, and its statistics can be a challenge to analyze. For example, using the nearest 24 observations to compute the RMSE means that the seasonal period that the RMSE is based on varies in a way that is difficult to predict. Also, RMSE has a minimum bound in the change test (referred to here as α_i), so it is not obvious to predict which factors affect the RMSE used in the final calculation.

In CCD-LCMAP, two calculations are performed across the full time series at the beginning of processing, for use in the change test. One, for each wavelength band, the minimum RMSE for the change test (α_i) is calculated. Two, the number and frequency of Landsat observations in the time series are used to determine the number of consecutive observations that will be needed in the change test to confirm a change detection (referred to here as the “peek number”). The peek number is effectively the sample size for the change detection test. The value of the peek number is at least six and increases in dense time series with frequent observations (Zhu et al., 2020).

Using the full time series for these calculations presents several potential complications. First, if there is a land cover change during the study period that substantially changes the reflectance behavior, α_i will depend on the behavior of both land covers. This has the potential to add undesirable variability; for example, the likelihood of detecting a fire event in 1990 could be affected by whether the location underwent development in 2000. Second, the behavior of the algorithm has the potential to differ when run across different time periods. Observation density roughly doubles after the launch of Landsat 7 in 1999, so the peek number calculation can be different depending on the time used. Ideally, adding more data at the end of the time series would not affect change detection early in the time series. Finally, use of full time series calculations adds implementation complications for forward processing. If new updates are to maintain consistency with previous data, α_i and the peek number need to be saved or recalculated during every update.

A.3. Calculation of the change test in CCD-BFP

The CCD-BFP change test is intended to address some of the challenges of the CCD-LCMAP change test described above, while not undermining its strengths. The change test in CCD-BFP has several differences from the CCD-LCMAP change test. First, the CCD-BFP change test is based only on data dated on or after the most recent detection of change, to avoid the conceptual and computational complications of potentially intermixing data from multiple land surface characteristics. All variable parameters are calculated at the time of the change test instead of using the full time series at the beginning of the procedure.

Let \mathbb{N} be the set of dates for the n observations in the fitted model. Expressing the fitted model (Eq. (A.1)) in matrix form,

$$\begin{bmatrix} \hat{y}_i(t_1) \\ \hat{y}_i(t_2) \\ \vdots \\ \hat{y}_i(t_n) \end{bmatrix} = \begin{bmatrix} 1 & t_1 & \cos \frac{2\pi t_1}{T} & \sin \frac{2\pi t_1}{T} & \cdots \\ 1 & t_2 & \cos \frac{2\pi t_2}{T} & \sin \frac{2\pi t_2}{T} & \cdots \\ \vdots & \vdots & \vdots & \vdots & \ddots \\ 1 & t_n & \cos \frac{2\pi t_n}{T} & \sin \frac{2\pi t_n}{T} & \cdots \end{bmatrix} \begin{bmatrix} c_{0i} \\ c_{1i} \\ a_{1i} \\ b_{1i} \\ \vdots \end{bmatrix} \quad (\text{A.3})$$

or $\widehat{y}_{i,\mathbb{N}} = X_{\mathbb{N}}c_i$, where \widehat{y}_i is the vector of predicted Landsat values for the i th band, $X_{\mathbb{N}}$ is the design matrix, and c_i is the vector of fitted coefficients for the i th band.

In CCD-BFP, the first data summarization is calculated per band, unlike CCD-LCMAP, where the first data summarization is calculated for each observation, across bands. The probability that all observations from \mathbb{M} (the set of dates to test for change) are consistent with the fitted model for the i th band ($p_i(\mathbb{M})$) is estimated from the test statistic

$$\frac{d_i^T [I + X_{\mathbb{M}} (X_{\mathbb{N}}^T X_{\mathbb{N}})^{-1} X_{\mathbb{M}}^T]^{-1} d_i}{s_i^2 m} \sim F(m, n - q) \quad (\text{A.4})$$

where $d_i = y_{i,\mathbb{M}} - \widehat{y}_{i,\mathbb{M}}$ is the vector of residuals, $X_{\mathbb{M}}$ is the design matrix for the set of observations to be tested, and s_i is the mean squared error for the fitted model. Eq. (A.4) follows the F -distribution, with q as the number of coefficients in c_i and $n - q$ as the degrees of freedom for the model (Chow, 1960). The term $X_{\mathbb{M}} (X_{\mathbb{N}}^T X_{\mathbb{N}})^{-1} X_{\mathbb{M}}^T$ in Eq. (A.4) incorporates consideration of the error in the model fit coefficients c_i , in addition to error in the new observations $y_{i,\mathbb{M}}$.

To summarize across the Landsat bands, CCD-BFP uses Fisher’s method of combining independent tests to estimate the probability that the observations in \mathbb{M} are consistent with the fitted models for all bands ($P(\mathbb{M})$):

$$-2 \sum_{i=1}^{\mu} \ln(p_i(\mathbb{M})) \sim \chi^2(2\mu) \quad (\text{A.5})$$

where $p_i(\mathbb{M})$ is calculated based on Eq. (A.4) and μ is the number of bands used for change detection. An implicit assumption in both this method and the CCD-LCMAP change test is that all the bands are independent, which is not the case. The CCD-BFP method has the possibility for approaches that account for non-independent bands, but here we use this approach for computational simplicity. All bands are available for all observations in the current study, and alternate approaches might be best evaluated in a study that combines multiple data sources (e.g., visible reflectance and synthetic aperture radar).

To address the challenge of outlier observations, the CCD-BFP method assumes that each observation has a probability λ of being an observation that should not be included in the change detection test. The probability that all observations are consistent with the model is then calculated as a weighted average of all possible subsets \mathbb{M} of the ℓ observations after date t :

$$P(t, \ell) = \sum_{\mathbb{M}} [(1 - \lambda)^m \lambda^{\ell - m} P(\mathbb{M})] \quad (\text{A.6})$$

where ℓ is the number of observations being tested for the detection of change (the “peek number” in CCD-LCMAP) and $P(t, \ell)$ is the estimated probability that there is a change that begins at time t . We use a probability cutoff of $P(t, \ell) < 10^{-10}$ to detect change, determined empirically to produce a similar number of change detections to CCD-LCMAP. We use a constant $\lambda = 0.05$ for CCD-BFP as a proof of concept, because extensive sensitivity testing of all parameters is beyond the scope of this work.

As in CCD-LCMAP, a change detection in CCD-BFP requires multiple observations to confirm change. Because the empty set is a subset of \mathbb{M} and $P(\mathbb{M}) > 0$, $P(t, \ell) > \lambda^\ell$, and thus a minimum number of observations must be examined to detect change in CCD-BFP. Change is flagged if $P(t, \ell) < 10^{-10}$, so the number of observations that must be examined to detect change is at least $8 \left(\frac{\log P(t, \ell)}{\log \lambda} = \frac{-10}{\log 0.05} \right)$. Increasing ℓ allows for the detection of lower magnitude change.

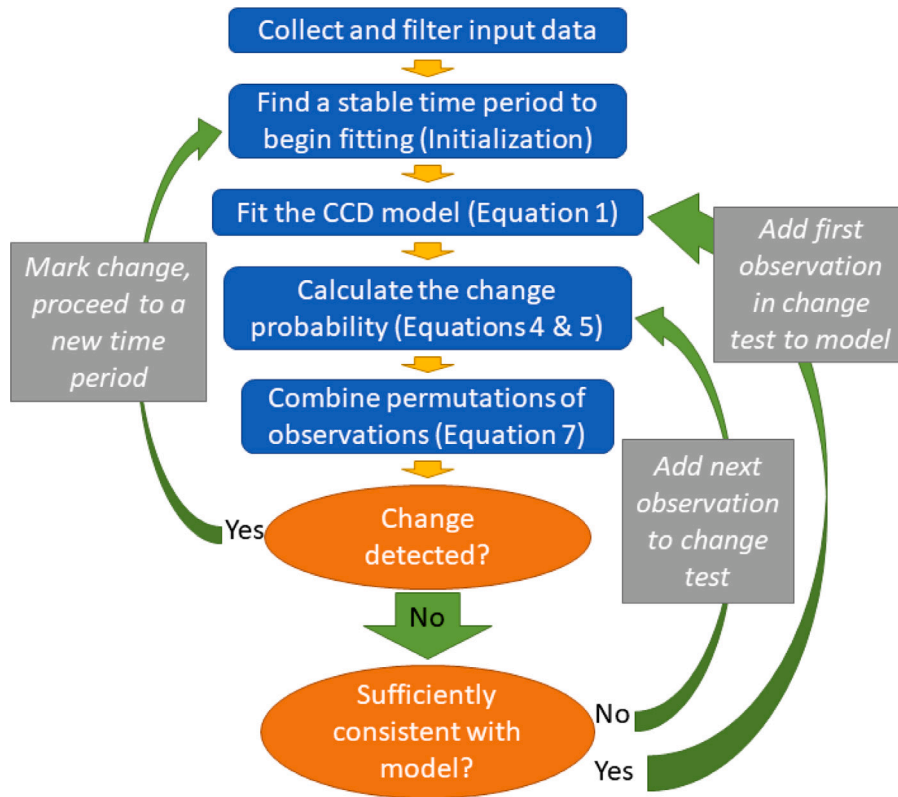


Fig. A.9. Flowchart for CCD-BFP algorithm.

Autocorrelation in the Landsat time series data has the potential to increase detection of change by CCD-BFP because the probability calculation above assumes that the new observations are independent. When observations are frequent, short periods of autocorrelation can increase detection of change, but when observations are less frequent, a reflectance difference needs to be long-lasting in order to lead to a change detection. To equalize across periods with different observation availability, in CCD-BFP Eq. (A.6) is modified to use only permutations where all new observations included in the calculation are separated by at least 10 days. Ten days was selected to incorporate at most one observation per cycle of Landsat acquisitions into the calculation of the change test while still utilizing all observations. The equation is

$$\begin{aligned}
 P(t, \ell) &= \frac{1}{P_{total}} \sum_{\mathbb{A}} (1 - \lambda)^a \lambda^{\ell - a} P(\mathbb{A}) \\
 P_{total} &= \sum_{\mathbb{A}} (1 - \lambda)^a \lambda^{\ell - a}
 \end{aligned}
 \tag{A.7}$$

where \mathbb{A} is a subset of the ℓ observations after date t such that no two observations are closer than 10 days apart and a is the number of observations in \mathbb{A} . Dividing by the total possible probability normalizes the final result to be within zero to one.

This approach to handling autocorrelation aims to reduce change detection in areas of short-term autocorrelation while still considering all new observations as part of the change test. It also performs the adjustment based on conditions at the time of the change test, so the adjustment will be appropriate for the actual number of observations available at the time of the change test. The number of days is targeted toward Landsat data availability to equalize toward the low end of the typical acquisition schedule. When there is only a single acquisition opportunity every 16 days, all observations will be included, but more frequent observations will be affected by this modification.

The CCD-BFP method uses a variable number of new observations to calculate the change test. The method begins by calculating the probability that the first new observation is consistent with the time series ($\ell = 1$). If the probability is below the cutoff threshold for

change, CCD-BFP will flag a change. If the probability is above a cutoff for no change, the change test will immediately stop and CCD-BFP will add it to the fitted model (Fig. A.9). If neither, CCD-BFP will proceed to run the change test for the first two observations ($\ell = 2$) and check again if the probability is low enough for change or high enough to stop the change test. The change test will continue to add observations until either the probability reaches one of the cutoffs, or the number of new observations reaches the cutoff peek number (18), in which case CCD-BFP will proceed with no change flagged. Computational approaches to this are described in Appendix D.

The CCD-BFP change test is designed to test if any new observations are different from their predicted values. This approach differs from the CCD-LCMAP change test, which is designed to test if all new observations are different from their predicted values. One advantage of the CCD-BFP change test is that if a few new observations are close to their predicted values, it is still possible to detect change when other new observations are sufficiently different. For example, a change that happens in the fall might be detected based on fall and spring observations even if a winter observation is similar to the predicted value. A major drawback of this CCD-BFP approach is that a change can be detected too soon if the first new observations are close to predicted, but later new observations are substantially different. The incremental approach described in the previous paragraph reduces the chance for change to be detected too soon because if the first new observation is highly consistent with the time series, no further new observations will be tested. However, if the first new observation is an outlier, it is possible to detect change too soon. To reduce this possibility, we added a routine after a change is detected to select the time of change. If an early peek observation is not very different from the model, while the final peek observations are above a threshold of difference, the change will be flagged starting at the first observation that exceeds the threshold.

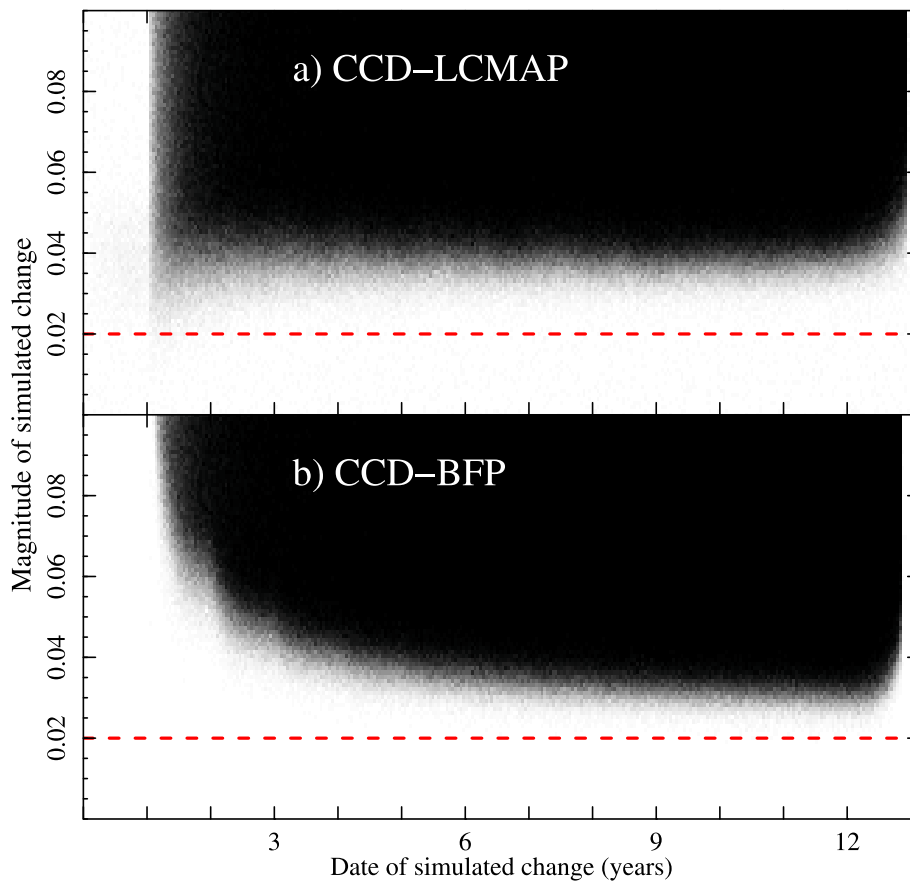


Fig. B.10. Change detection sensitivity for simulated data that has a simulated change, for (a) CCD-LCMAP and (b) CCD-BFP. Each shaded pixel in the image shows the fraction of 100 simulated time series that had change detected by CCD, with black pixels having 100% of simulated time series with a change detection by CCD, and 0% for white pixels. Timing of the simulated change is shown on the x -axis, and magnitude of the simulated change is shown on the y -axis. Red dotted lines show the standard deviation of the simulated noise in the time series data. (For interpretation of the references to color in this figure legend, the reader is referred to the web version of this article.)

Appendix B. Extended results

Simulated data were also useful for demonstrating the sensitivity of the CCD-LCMAP and CCD-BFP methods. Both methods had nearly 100% detection rates for change with a change magnitude more than three times the standard deviation of the noise and after 2 years of elapsed time (Fig. B.10). The sensitivity was relatively even through time for CCD-LCMAP, while CCD-BFP sensitivity to lower magnitude change increased throughout the 13 years of simulated data. With CCD-LCMAP, there were a few scattered detections of change for lower magnitude changes and a few detections when the simulated change preceded the earliest date of change CCD is expected to detect (1 year elapsed time). With CCD-BFP, a reduction in sensitivity was noticeable just before two years of elapsed time, and just before three years of elapsed time. Neither method detected change near the end of the time series, when not enough data remained, and both methods had reduced detection at low change magnitudes near the cutoff time.

We additionally made qualitative observations during the evaluation change detection by CCD-BFP. Although we have not performed quantitative work to support these observations, they are potentially of interest. The results of the qualitative analysis follow:

- In areas that were developed during the study period, change detection performed reasonably well in locations that were previously forest, but development from cropped land was not well captured in either CCD-LCMAP or CCD-BFP, with the possibility that results were worse for CCD-BFP than for CCD-LCMAP. The surface reflectance of cropped area can be highly variable so it is especially difficult to detect change.

- Qualitatively, we observed a few instances where destruction from wind events in northern CONUS were not well captured in CCD-LCMAP but were detected by CCD-BFP. Although these types of events represent only a small fraction of change, they are relatively easy to interpret qualitatively so improvement indicates that additional isolated improvements in results are plausible.
- Although change detections were reduced in CCD-BFP relative to CCD-LCMAP for drought-affected locations in the Great Plains, there appeared to be increased drought-related change detections in areas of the southwestern United States. These locations have more shrub land cover than the Great Plains and might see longer persistence of drought impacts. The increased detections in CCD-BFP sometimes produced notable SLC artifacts in swath overlap areas.

Table B.3 is similar to Table 1 but with additional results from CCD-BFP with different change threshold values.

Appendix C. Cumulative calculation of CCD-BFP

A major goal of the CCD methodology is continuous updating, such that results can be updated based on additional data at the end of the time series without affecting results earlier in the time series. Continuous calculation is desirable for rapid and frequent (i.e., on the order of days) updating of change detection results. Conceptually, all versions of CCD (i.e., since Zhu and Woodcock (2014)) support this goal, but several implementation challenges produce complications.

One challenge is that the CCD-LCMAP method requires that the majority of the Landsat archive be read every time an update is desired.

Table B.3

Number of changes in the validation dataset detected (± 1 year) by CCD-BFP using varying thresholds for the probability cutoff.

Threshold	CCD-BFP											Validation
	10 ⁻⁵	10 ⁻⁶	10 ⁻⁷	10 ⁻⁸	10 ⁻⁹	10 ⁻¹⁰	10 ⁻¹¹	10 ⁻¹²	10 ⁻¹³	10 ⁻¹⁴	10 ⁻¹⁵	
Harvest	901	889	859	844	822	791	770	732	696	665	608	1048
Mechanical	261	258	247	231	225	211	209	198	179	164	151	332
Fire	154	147	148	142	137	134	126	121	106	95	88	184
Hydrology	63	63	62	57	52	51	46	42	41	37	31	77
Wind	12	13	12	11	11	11	9	9	9	9	8	14
Other	714	683	640	584	526	470	418	366	310	271	217	796
Structural decline	176	174	164	150	142	133	120	105	97	93	82	223
Growth/recovery	2136	1868	1592	1423	1298	1184	1103	1022	956	899	846	2910
Total changes	21929	14716	10301	7437	5593	4312	3432	2789	2354	2009	1682	
Changes 1985–2012	18397	12433	8756	6351	4783	3706	2971	2415	2046	1760	1484	
Matched (1985–2012)	4530	3800	3270	2776	2413	2133	1868	1677	1510	1357	1158	

If any of the input data have been modified or are no longer available, there will be complications with how to treat results and operational inconsistencies. Reading the full archive for every update also presents potential operational obstacles to frequent updating or spatial processing. Also, the difficulty of reading the full archive increases through time as the archive gets larger and could especially be more challenging if additional data sources (e.g., Sentinel-2) are added to the process.

Another challenge is that running the model-fitting procedure from scratch becomes more computationally expensive as the model increases in length. In CCD-LCMAP, the model is re-fit only after 33% more time is added to the time series, partly in order to reduce this computational load. Reducing the computation required is desirable to remove a constraint on algorithm development as well as to reduce the processing required.

In CCD-BFP, we approach these challenges by accumulating intermediate matrix products outside the fitting procedure. The current CCD-BFP implementation only uses these matrices to speed calculation, but they might also be used to reduce or eliminate the need to read the full archive for an update by saving between update runs.

Variables used in this section follow those used in Appendix A. Let Y be the n -by- μ matrix of the n Landsat observations in the current fitted model and the μ bands used for change detection. The three arrays that are stored are the q -by- q matrix $X^T X$ (the Gram matrix), the q -by- μ matrix $X^T Y$, and the μ values $y_i \cdot y_i$. These can be computed incrementally, for example

$$y_{i, \{N, N+1\}} \cdot y_{i, \{N, N+1\}} = y_{i, N} \cdot y_{i, N} + (y_i(t_{N+1}))^2 \quad (C.1)$$

When n is large, this can produce substantial computational savings.

OLS regression is used in CCD-BFP, so the coefficient vector c_i can be solved from $X^T X$ and $X^T y_i$ using Cholesky factorization. In CCD-LCMAP and most other implementations of CCD, LASSO is used for fitting the model. The LASSO c_i vector can be calculated using $X^T X$, $X^T y_i$, and $y_i \cdot y_i$, so this approach to reducing computation is also possible for other versions of CCD.

The sum of squared residuals is used in both CCD-LCMAP and CCD-BFP, and also can be calculated from these arrays.

$$s_i^2 = y_i \cdot y_i + c_i \cdot (-2X^T y_i + X^T X c_i) \quad (C.2)$$

To show this, let x_{kj} be the j th value in $X_{\{t_k\}}$ (element (k, j) in X), c_{ji} be the j th coefficient in c_i , and $y_{ki} = y_i(t_k)$.

$$\begin{aligned} s_i^2 &= \sum_{k=1}^n (y_{ki} - \widehat{y}_{ki})^2 \\ &= \sum_{k=1}^n \left(y_{ki} - \sum_{j=1}^q c_{ji} x_{kj} \right)^2 \\ &= \sum_{k=1}^n y_{ki}^2 - 2 \sum_{k=1}^n \left(y_{ki} \sum_{j=1}^q c_{ji} x_{kj} \right) + \sum_{k=1}^n \left[\left(\sum_{j=1}^q c_{ji} x_{kj} \right) \left(\sum_{\ell=1}^q c_{\ell i} x_{k\ell} \right) \right] \\ &= \sum_{k=1}^n y_{ki}^2 - 2 \sum_{j=1}^q \left(c_{ji} \sum_{k=1}^n y_{ki} x_{kj} \right) + \sum_{j=1}^q \left[c_{ji} \sum_{\ell=1}^q \left(c_{\ell i} \sum_{k=1}^n x_{kj} x_{k\ell} \right) \right] \end{aligned}$$

$$= y_i \cdot y_i + c_i \cdot (-2X^T y_i + X^T X c_i) \quad (C.3)$$

In CCD-BFP, the test statistic for change detection (Eq. (A.4)) requires only $X_N^T X_N$, c_i , and s_i from the time range of the fitted model (\mathbb{N}). This means it is possible to compute the change test in CCD-BFP based only on the values in $X^T X$, $X^T Y$, and $y_i \cdot y_i$ (plus X_M and Y_M for the observations after the end of the fitted model). In CCD-LCMAP, the root mean squared error for the nearest 24 observations (by day of year) is used as part of the change detection test, and this value is not calculated based on the incremented arrays, although those arrays can still be used in CCD-LCMAP to reduce the computational overhead of frequent model refitting.

These calculations are potentially subject to catastrophic cancellation, but in CCD-BFP the number of observations is relatively modest (on the order of thousands) and the values in X and Y are of a somewhat similar order of magnitude even without centering. CCD-BFP utilizes 64-bit floats but does not otherwise account for numerical round-off. Additional consideration might be required for substantially increased numbers of observations or different models X .

Appendix D. Computation of CCD-BFP change test

The CCD-BFP change test accounts for the possibility of cloud or other problem observations by combining the probabilities of multiple permutations of the new “peek” observations. The CCD-BFP change test iterates across the new observations (values of ℓ), as described in Appendix A.3. In many cases CCD-BFP will only require a small value of ℓ to reject the possibility of a change at the current date t , but when larger values of ℓ are required, the computational burden becomes prohibitive. We reduce the computation required by first calculating the probability $P(\mathbb{A})$ for the subset \mathbb{A} with all ℓ observations, then the subsets \mathbb{A} with $a = \ell - 1$ observations, then $a = \ell - 2$, etc. Subsets with large a will have the largest weights $(1 - \lambda)^a \lambda^{\ell - a}$. After all permutations for a value of a are calculated, we calculate the probabilities

$$\begin{aligned} P_{min}(t, \ell, \psi) &= \frac{1}{P_{total}} \sum_{\mathbb{A} | a \geq \psi} (1 - \lambda)^a \lambda^{\ell - a} P(\mathbb{A}) \\ P_{max}(t, \ell, \psi) &= \frac{1}{P_{total}} \left(\sum_{\mathbb{A} | a \geq \psi} (1 - \lambda)^a \lambda^{\ell - a} P(\mathbb{A}) + \sum_{\mathbb{A} | a < \psi} (1 - \lambda)^a \lambda^{\ell - a} \right) \end{aligned} \quad (D.1)$$

where ψ is the current minimum a that has been computed. $P(t, \ell) \leq P_{max}(t, \ell, \psi)$, so if $P_{max}(t, \ell, \psi)$ is below the change threshold, CCD-BFP flags a change for this date t . $P(t, \ell) \geq P_{min}(t, \ell, \psi)$, so if $P_{min}(t, \ell, \psi)$ is above the change threshold, it is not possible to have a change for this value of ℓ , and CCD-BFP proceeds to test the next value of ℓ without calculating smaller values of ψ . In addition, if $P_{min}(t, \ell, \psi)$ is above a higher threshold, CCD-BFP will assume there is no change at this date t and proceed to the next date without calculating larger values of ℓ for this date.

References

- Auch, R.F., Wellington, D.F., Taylor, J.L., Stehman, S.V., Tollerud, H.J., Brown, J.F., Loveland, T.R., Pengra, B.W., Horton, J.A., Zhu, Z., Midekisa, A.A., Saylor, K.L., Xian, G., Barber, C.P., Reker, R.R., 2022. Conterminous United States land-cover change (1985–2016): New insights from annual time series. *Land* 11, <http://dx.doi.org/10.3390/land11020298>.
- Bezanson, J., Edelman, A., Karpinski, S., Shah, V.B., 2017. Julia: A fresh approach to numerical computing. *SIAM Rev.* 59, 65–98. <http://dx.doi.org/10.1137/141000671>.
- Brown, J.F., Tollerud, H.J., Barber, C.P., Zhou, Q., Dwyer, J.L., Vogelmann, J.E., Loveland, T.R., Woodcock, C.E., Stehman, S.V., Zhu, Z., et al., 2020. Lessons learned implementing an operational continuous United States national land change monitoring capability: The land change monitoring, assessment, and projection (LCMAP) approach. *Remote Sens. Environ.* 238, 111356. <http://dx.doi.org/10.1016/j.rse.2019.111356>.
- Chow, G.C., 1960. Tests of equality between sets of coefficients in two linear regressions. *Econometrica* 28, 591–605. <http://dx.doi.org/10.2307/1910133>.
- Cohen, W.B., Yang, Z., Stehman, S.V., Schroeder, T.A., Bell, D.M., Masek, J.G., Huang, C., Meigs, G.W., 2016. Forest disturbance across the conterminous United States from 1985–2012: The emerging dominance of forest decline. *For. Ecol. Manag.* 360, 242–252. <http://dx.doi.org/10.1016/j.foreco.2015.10.042>, special Section: Forest Management for Climate Change.
- Dwyer, J.L., Roy, D.P., Sauer, B., Jenkerson, C.B., Zhang, H.K., Lyburner, L., 2018. Analysis ready data: Enabling analysis of the landsat archive. *Remote Sens.* 10, <http://dx.doi.org/10.3390/rs10091363>, <https://www.mdpi.com/2072-4292/10/9/1363>.
- Egorov, A.V., Roy, D.P., Zhang, H.K., Li, Z., Yan, L., Huang, H., 2019. Landsat 4, 5 and 7 (1982 to 2017) analysis ready data (ARD) observation coverage over the conterminous united states and implications for terrestrial monitoring. *Remote Sens.* 11, <http://dx.doi.org/10.3390/rs11040447>.
- Gómez, C., White, J.C., Wulder, M.A., 2016. Optical remotely sensed time series data for land cover classification: A review. *ISPRS J. Photogramm.* *Remote Sens.* 116, 55–72. <http://dx.doi.org/10.1016/j.isprsjprs.2016.03.008>.
- Pengra, B., Stehman, S., Horton, J., Dockter, D., Schroeder, T., Yang, Z., Hernandez, A., Healey, S., Cohen, W., Finco, M., Gay, C., Houseman, I., 2021. LCMAP reference data product 1984–2018 land cover, land use and change process attributes (ver. 1.2). <http://dx.doi.org/10.5066/P9ZWOXJ7>.
- QGIS Development Team, 2016. QGIS Geographic Information System. Open Source Geospatial Foundation Project, <http://qgis.osgeo.org>.
- U.S. Geological Survey, 2018. Landsat WRS 2 ascending path row shapefile. <https://www.usgs.gov/media/files/landsat-wrs-2-ascending-path-row-shapefile>.
- U.S. Geological Survey, 2020a. Land Change Monitoring, Assessment, and Projection (LCMAP) Continuous Change Detection and Classification (CCDC) Algorithm Description Document (ADD). Technical Report LSDS-1982, U.S. Geological Survey, Sioux Falls, South Dakota, <https://www.usgs.gov/media/files/lcmap-ccdc-add>.
- U.S. Geological Survey, 2020b. LCMAP collection 1.0 science products. <http://dx.doi.org/10.5066/P9W1T06E>.
- U.S. Geological Survey, 2020c. U.S. Landsat Collection 1 (C1) Analysis Ready Data (ARD) Data Format Control Book (DFCB). Technical Report LSDS-1873, U.S. Geological Survey, Sioux Falls, South Dakota, <https://www.usgs.gov/media/files/landsat-analysis-ready-data-ard-data-format-control-book-dfcb>.
- U.S. Geological Survey, 2021. Monitoring trends in burn severity national burn severity mosaics. <https://www.mtbs.gov>. (Accessed 30 June 2021).
- USGS Advanced Research Computing, 2022. USGS denali supercomputer: U.S. Geol. Surv. <http://dx.doi.org/10.5066/P9PSW367>.
- Woodcock, C.E., Loveland, T.R., Herold, M., Bauer, M.E., 2020. Transitioning from change detection to monitoring with remote sensing: A paradigm shift. *Remote Sens. Environ.* 238, 111558. <http://dx.doi.org/10.1016/j.rse.2019.111558>.
- Wulder, M.A., Coops, N.C., Roy, D.P., White, J.C., Hermosilla, T., 2018. Land cover 2.0. *Int. J. Remote Sens.* 39, 4254–4284. <http://dx.doi.org/10.1080/01431161.2018.1452075>.
- Xian, G.Z., Smith, K., Wellington, D., Horton, J., Zhou, Q., Li, C., Auch, R., Brown, J.F., Zhu, Z., Reker, R.R., 2022. Implementation of the CCDC algorithm to produce the LCMAP collection 1.0 annual land surface change product. *Earth Syst. Sci. Data* 14, 143–162. <http://dx.doi.org/10.5194/essd-14-143-2022>.
- Zhu, Z., Woodcock, C.E., 2014. Continuous change detection and classification of land cover using all available Landsat data. *Remote Sens. Environ.* 144, 152–171. <http://dx.doi.org/10.1016/j.rse.2014.01.011>.
- Zhu, Z., Woodcock, C.E., Holden, C., Yang, Z., 2015. Generating synthetic Landsat images based on all available Landsat data: Predicting Landsat surface reflectance at any given time. *Remote Sens. Environ.* 162, 67–83. <http://dx.doi.org/10.1016/j.rse.2015.02.009>.
- Zhu, Z., Zhang, J., Yang, Z., Aljaddani, A.H., Cohen, W.B., Qiu, S., Zhou, C., 2020. Continuous monitoring of land disturbance based on Landsat time series. *Remote Sens. Environ.* 238, 111116. <http://dx.doi.org/10.1016/j.rse.2019.03.009>.